Research Article Vol. 27, No. 5 | 4 Mar 2019 | OPTICS EXPRESS 6030

Optics EXPRESS

Ultrafast x-ray absorption near edge spectroscopy of Fe_3O_4 using a laboratory based femtosecond x-ray source

M. I. Anwar,[1] M. Iqbal,[2] B. J. Hwang,[1] M. Faiyaz,[1] B. S. Mun,[1] K. A. Janulewicz,[3] and D. Y. Noh[1,*]

[1] *Department of Physics and Photon Science, Gwangju Institute of Science and Technology, Gwangju, South Korea*
[2] *National Institute of Lasers and Optronics, Islamabad, Pakistan*
[3] *Military Institute of Technology, Warsaw, Poland*
[*] *dynoh@gist.ac.kr*

Abstract: An ultrafast time-resolved x-ray absorption near edge spectroscopy (XANES) experiment was performed on a magnetite (Fe_3O_4) film using a femtosecond laser plasma x-ray source delivering Bremsstrahlung radiation. Ultrafast temporal evolution of the XANES of Fe_3O_4 following an excitation by an infra-red (IR) laser pulse was observed in a pump-probe scheme. The Fe K x-ray absorption edge shifts towards low energy upon IR excitation as much as 12 eV, which is mainly attributed to the charge transfer between the Fe ions. The shift in the absorption edge occurred within about 150 fs, a typical time of non-thermal electronic redistribution. The charge transfer also causes an ultrafast increase in the IR transmission in a similar time scale.

1. Introduction

Magnetite (Fe_3O_4) has attracted much interest due to its rich magnetic and transport properties [1]. It is one of the most studied oxides in relation to insulator to metal transition and also has vast applications in oxide electronics and memory devices [2–5]. Magnetite has an inverse cubic spinel structure in which tetrahedrally coordinated A-sites are occupied solely by Fe^{3+} ions, while octahedrally coordinated B-sites are occupied by an equal number of Fe^{3+} and Fe^{2+} ions. Magnetite is in ferromagnetic semi-metallic phase at room temperature. For future applications of Fe_3O_4 in high speed devices, understanding ultrafast behaviors of its electronic and lattice structure is on demand. Ultrafast demagnetization in Fe_3O_4 nanocrystals upon optical excitation was investigated by Faraday rotation measurements [6]. Ultrafast infrared (IR) transmission in the insulating and semimetallic phase below and above Verwey transition exhibits distinct differences [7].

The third generation synchrotrons and x-ray free electron lasers (XFEL) have extended materials research in static to dynamic domain utilizing ultrashort x-ray pulses, which has facilitated deeper understanding of chemical reaction dynamics [8], non-thermal melting [9], electron dynamics in metals [10]. Typically, specimens are excited by an ultrashort laser pulse and subsequently probed with an ultrashort x-ray pulse at a specific delay that can reveal atomic scale dynamics. These large scale facilities, however, have major disadvantage in their accessibility and inherent difficulties in synchronizing probe x-ray and pump IR beams which are independently controlled. In the meanwhile, tremendous progresses have been achieved on laboratory-scale laser plasma X-ray sources (LPXS) driven by intense but compact femto-second lasers during last decade [11–14]. Sub-picosecond pulse duration and reasonable flux of LPXSs are available due to the high repetition femtosecond lasers of milli-joule (mJ) energy. A variety of interesting time-resolved x-ray absorption spectroscopy and x-ray diffraction experiments have been reported using LPXS [15–18]. Femtosecond LPXSs offer a unique opportunity to study the electronic

#351316 https://doi.org/10.1364/OE.27.006030
Journal © 2019 Received 7 Nov 2018; revised 12 Jan 2019; accepted 6 Feb 2019; published 20 Feb 2019

rearrangements on their natural ultrafast time scales that are not reachable using typical analytic methods.

In this paper, we report an ultrafast pump-probe x-ray absorption spectroscopy results on magnetite (Fe_3O_4) by using a LPXS. We found that the Fe K-absorption edge in Fe_3O_4 red-shifts under IR pumping, which was attributed to ultrafast charge transfer between Fe ions.

2. Experimental setup

Figure 1 shows the pump-probe LPXS XANES measurement scheme used in this work. Intense IR laser pulses with 50 fs pulse width and 4.5 mJ energy centered at a wavelength of 800 nm generated from a Ti: Sapphire laser with a 1 kHz repetition rate was focused to a Cu tape target to generate laser plasma x-rays. The Cu target and the optical elements were installed in a chamber at a pressure of $\sim 10^{-3}$ torr. The laser beam was focused to a diameter of 8 μm and intensity of 10^{17} W/cm^2 was achieved by using an off axis parabolic mirror, and hard x-rays were generated as a result of intense laser matter interaction. For the time resolved pump-probe XANES measurements, about 70% of the main IR laser beam was used for x-ray generation and the remaining 30% was split and delayed to use as an excitation pump pulse. The delay between the IR pump and x-ray probe beam arrival times can be controlled precisely, because both the pump and probe beams are generated using a single laser source. For pump-probe XANES measurements, the x-ray and laser pulse were overlapped spatially on the specimen. Pump IR beam was directed to the sample at normal incidence covering whole area of a specimen. The angle between the pump and probe beams was maintained below 10^o to reduce the temporal elongation which is introduced by the angular difference. X-rays transmitted through the specimen was directed to a cylindrically bent, highly annealed pyrolytic graphite (HAPG) crystal spectrometer in the point-to-point focusing in Von Hamos arrangement [19]. The small mosaicity of the HAPG crystal of about 0.11^o limited the effective aperture of the sample and minimized the spread in probe beam arrival time. A normalization scheme was developed in which the sample signal and the monitor signal can be measured simultaneously in order to overcome the inherent source intensity fluctuations. For precise energy calibration at each delay, the Cu K-alpha lines were measured together with the Fe K -edge simultaneously. The energy resolution of the current set up including the drift in the energy calibration point caused by various fluctuations in the optical elements was about 1.5 eV. Details of the LPXS and the XANES setup were reported previously [20].

In addition to the IR pump X-ray probe measurements, we carried out an IR pump IR probe

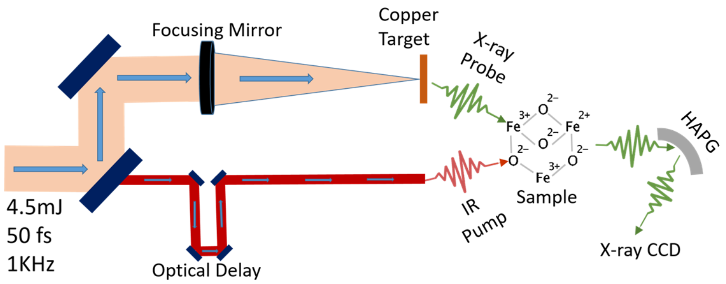

Fig. 1. Schematic diagram of the pump-probe XANES measurement setup using a laser plasma x-ray source.

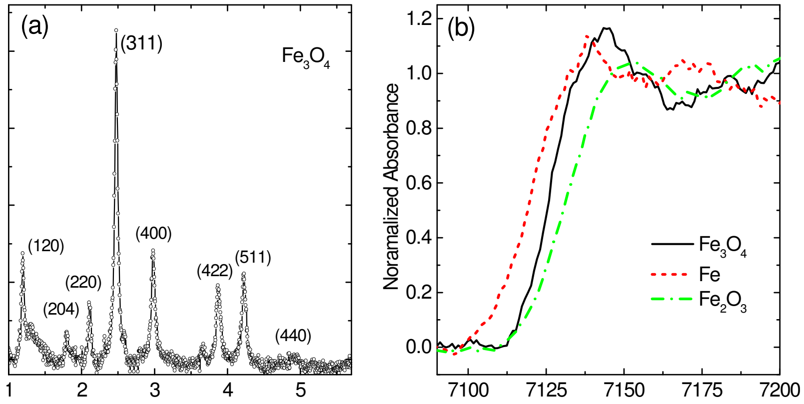

Fig. 2. (a) X-ray diffraction profile of the Fe_3O_4 film grown by the sputtering method used in the experiment. The solid line is a guide-to-eye. (b) XANES spectrum of the Fe_3O_4 specimen shown together with the spectra of Fe and Fe_2O_3 for comparison obtained using the LPXS setup.

measurement with the same laser system. The pump IR beam in this case was focused to a spot size of 1 mm and neutral density filters were used in order to avoid the damage due to the IR fluence. The pump beam was changed from the p-polarized to s-polarized with the half wave plate in order to avoid the coherent artifact effect. For this measurement, a 500 nm thick Fe_3O_4 sample was used. The sample was excited with a pump fluence of 10 to 20 mJ/cm^2 and the change in the IR transmission was recorded using a photo diode spectrometer.

A 4 μm thick Fe_3O_4 film investigated in this study was deposited on a polyimide film by radio-frequency magnetron sputtering of a Fe_3O_4 powder target. The distance between the powder target and substrate was kept at 35 mm. The sputtering chamber was evacuated to 5×10^{-6} torr prior to the deposition. Flow rate of Ar was kept at 20 sccm, maintaining the working pressure of 5×10^{-3} torr during deposition, and the growth temperature was about 500^oC. The Fe_3O_4 specimens were characterized by x-ray diffraction at the 5D beamline at Pohang light source, as shown in Fig. 2(a). The peak positions and the intensity ratios of the Bragg reflections match well with the reported values of magnetite. The XANES spectrum near the Fe K-absorption edge of the Fe_3O_4 specimen was also compared to that of metallic Fe and Fe_2O_3 measured in the same set up in Fig. 2(b). These spectra are in agreement with the available data in the literature in terms of the edge positions, although the detailed features of the spectra are somewhat smeared out due to the limited flux and finite energy resolution. The clear difference in the absorption edge position in the three specimens, however, confirms that the energy resolution of the spectrometer is sufficient to resolve the change in the oxidation state of Fe ions.

3. Results and discussion

Shown in Fig. 3(a) are the normalized pump-probe XANES spectra of the Fe_3O_4 before and after the arrival of pump IR beam at 15 mJ/cm^2 together with unpumped cold spectrum. Each normalized absorption spectrum was extracted from the measured transmitted x-ray intensity following the standard data-reduction procedure (ATHENA) used in XANES analysis [21]. It took about 2 hours to accumulate enough statistics for each spectrum at a given delay. In the XANES spectrum measured 965 fs prior to the arrival of the pump IR beam, the Fe-K edge occurs around 7126 eV, which is about 1 eV smaller than the edge position of the cold Fe_3O_4 specimen without pumping. They are practically the same, and the difference was due to the

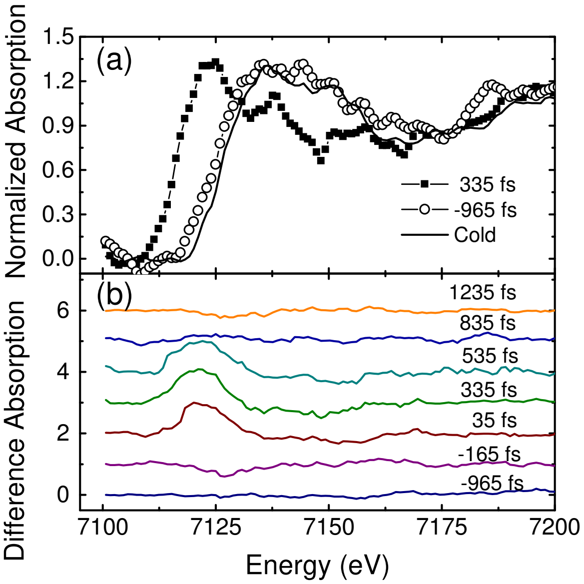

Fig. 3. (a) XANES spectra of Fe_3O_4 measured at 965 fs prior to arrival of the pump and 335 fs after the pump beam. A spectrum of the cold unpumped sample is also included as a reference. The data are normalized following the standard procedure for XANES spectra. (b) Difference XANES spectra at various delays obtained from the normalized XANES spectrum at each delay subtracted by the cold spectrum.

drift in the energy calibration point. At the delay after pumping approaches to 335 fs, however, the K-absorption edge shifts towards the low energy side and occurs at around 7116 eV, about 10 eV less than the cold sample. We note that the zero of the delay time was determined to be the beginning of the shift in the K-edge. Shown in Fig. 3(b) are the difference between the spectrum measured at each delay and the cold spectrum. They are the same data used in Fig. 3(a) but exhibit the evolution of the spectrum more clearly. The XANES spectra at 335 and 535 fs significantly deviate from the cold spectrum and return back to the cold one as the delay time increases above 800 fs. The detailed structure other than the edge position in the XANES spectra , however, was difficult to analyze due to insufficient statistics of the low flux LPXS.

The behavior of the Fe K x-ray absorption edge as a function of the delay time is illustrated in Fig. 4, in which the maximum position in the first derivative of the XANES curve at each delay are displayed. We fit the initial decreasing and recovery region to an error function and an exponential respectively. The zero of time delay was indeed chosen to be the beginning of the change in XANES curve determined by fitting the initial decreasing part to an error function. The amount of the redshift was as much as 12±3 eV which can be clearly resolved in the current LPXS based XANES setup. The width in the error function (2σ), which we attribute to the time resolution of this measurement, was about 150 fs, and the time constant in the exponential recovery part was about 500 fs. Due to the limited number of the data point, however, the reliability in time constants is rather low, and it is more meaningful to discuss the total duration of the redshift, ~ 690 fs, indicated by an arrow in the Fig. 4.

Prior to the pump probe XANES measurement, we also carried out a time resolved IR transmission measurement upon IR pumping in a similar experimental setup as the one used in the XANES measurement. The reason for this one color IR transmission measurement was to find the sample response to IR excitation and to determine a suitable pump fluence level for the pump-probe XANES measurements, rather than detailed IR spectrum analysis. Figure 5 shows

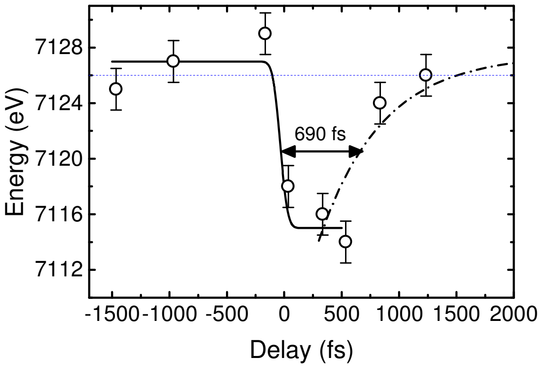

Fig. 4. Behavior of Fe K absorption edge obtained from the XANES curves. The solid line is a result of fitting the initial decreasing part to an error function, and the dotted line is a fit of the recovery part to an exponential. Dotted line indicates the K-edge position of cold Fe_3O_4 .

the behavior of IR transmission before and after the IR pumping with a fluence from 10 mJ/cm^2 to 20 mJ/cm^2 as a function of the delay time. The IR transmission increases instantaneously and recovered to the cold value in about 380 fs. The amount of the reduction in absorption increases with the pumping power which saturates around 20 mJ/cm^2. The time constant involved in the IR absorption is smaller than the x-ray absorption edge position shown in Fig. 3(b), which we attribute to the increased time resolution by the x-ray generation process and the time elongation by the angular difference in the pump IR and probe X-ray beam as mentioned in the experimental setup part. Both the behavior in the XANES and IR transmission are likely to be caused by a same physical origin.

Optical absorption observed in Fe_3O_4 has often been attributed to various intervalence charge

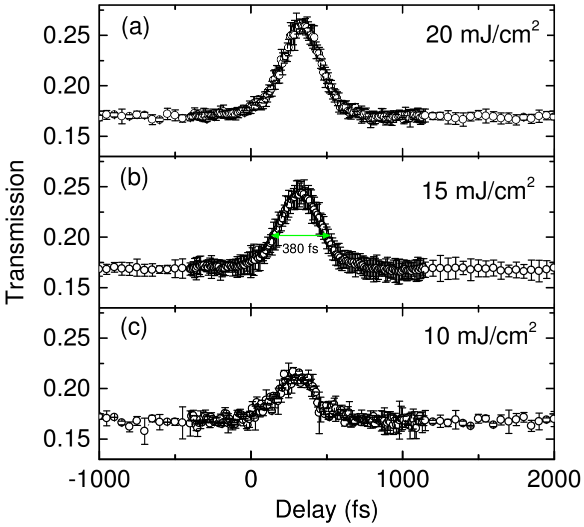

Fig. 5. IR Transmission through a 500 nm thick Fe_3O_4 film as a function of the delay. It is excited by 800 nm IR pulses at fluence of 20 mJ/cm^2 (a), 15 mJ/cm^2 (b), and 10 mJ/cm^2 (c).

transfer (IVCT) among Fe^{2+} and Fe^{3+} ions located in the octahedral and tetrahedral sites occurring at 0.56, 1.94, 3.11, and 3.94 eV [23, 24]. Since the energy of IR pump beam used in this experiment was 1.55 eV, we conjecture that the transfer at 3.11 eV through two photon absorption process contributes mostly to the observed behavior, which is consistent to the fact that our pump beam is rather intense. The IR pump beam depletes the possible absorption routes of IVCT which can lead to increase in the transmission of the probe IR beam. The electron transfer from oxygen ions is not likely to happen since the oxygen p-state is rather far from the Fermi level. The time scale of the change in our IR transmission is consistent to that the IVCT which is an electronic process occurring in much faster time scale then lattice motion [22]. A similar ultrafast change in the IR absorption in Fe_3O_4 films have been reported under ultraviolet pumping with much smaller power and was attributed to the momentary exhibition of metallic behavior in semimetallic magnetite [7].

The change in the 3d valence electron distribution around the Fe^{2+} and Fe^{3+} ions caused by IR pumping would influence the ionization energy of the 1s electron and the energy required to add an electron to 4p state [25]. This results in the change of the Fe K x-ray absorption edge representing mostly the 1s to 4p transition. The enhancement of the pre-edge excitations of 1s electrons to the vacant 3d levels generated during the pumping may also contribute to the redshift as the parity selection rule is relaxed for the intersite transitions, but we think that it is not the major cause. Chen *et. al.* reported a similar amount of redshift (~ 10 eV) in the Fe edge in ferrioxalates under IR pumping in a time resolved extended x-ray absorption spectroscopy study, although their focus was the structural change of the Fe-O bond distance rather than the edge shift [26]. The large redshift observed at the Fe K-edge position during IR pumping is reminiscence of the chemical shift due to the reduction of Fe ions. Typically, Fe K-edge exhibits significant redshift as the oxidation number of Fe ions reduces. It is, therefore, reasonable to attribute the observed redshift in Fe_3O_4 to the effective chemical shift caused by the charge transfer during optical excitation. Quantitative description, however, requires more experimental measurements and theoretical calculations.

4. Conclusion

Ultrafast transient XANES of a magnetite Fe_3O_4 are measured near the Fe K-edge region using a high resolution HAPG spectrometer based on a LPXS in a pump-probe scheme. The IR pumped magnetite exhibits a red shift in the Fe K x-ray absorption edge in about 150 fs and recovered in 500 fs. The cause of the redshift is attributed to the change in the 3d valence electron distribution of Fe ions. IR transmission also increases momentarily by the IR excitation consistent with the behavior of x-ray absorption. This work demonstrated that ultrafast XANES based on LPXSs is a powerful tool to probe fast electronic processes occurring in transition metal oxides.

Funding

National Research Foundation of Korea (NRF)(2015R1A5A1009962,2016R1A6B2A02005471); GIST Project 2019; Ministry of Science and ICT of Korea (Pohang Light Source).

Acknowledgments

We gratefully acknowledge H. Stiel and P. V. Nickles for their contribution in setting up the laser plasma x-ray source.

References

1. G. Zhang, C. Fan, L. Pan, F. Wang, P. Wu, H. Qiu, “Magnetic and transport properties of magnetite thin films," J. Magn. Magn. Mater. **239**, 737–745 (2005).
2. Y. Jiang, T. Lee, W. Li, G. Ketwaroo, C. G. Rose-Petruck, “High-average-power 2-kHz laser for generation of ultrashort x-ray pulses," Opt. Lett. **27**, 963-965 (2002).

3. A. Oguz Er, J. Chen, P. M. Rentzepis, “Ultrafast time resolved x-ray diffraction, extended x-ray absorption fine structure and x-ray absorption near edge structure," J. Appl. Phys. **112**, 031101 (2012).
4. F. Dorchies, A. Lévy, C. Goyon, P. Combis, D. Descamps, “Unraveling the solid-liquid-vapor phase transition dynamics at the atomic level with ultrafast X-ray absorption near-edge spectroscopy," Phys. Rev. Lett. **107**, 245006 (2011).
5. H. Nakano, Y. Goto, P. Lu, T. Nishikawa, “Time-resolved soft x-ray absorption spectroscopy of silicon using femtosecond laser plasma x rays," Appl. Phys. Lett. **75**, 2350–2352 (1999).
6. C. H. Hsia, T. Y. Chen, D. H. Son, “Size-dependent ultrafast magnetization dynamics in iron oxide (Fe_3O_4) nanocrystals," Nano. Lett. **8**, 571–576 (2008).
7. A. Mokhtari, J. R. Neal, H. J. Blythe, “Ultra-fast spectroscopy investigation of Verwey transition in magnetite," Iranian Journal of Physics Research **15**, 345 (2015).
8. S. Fourmaux, L. Lecherbourg, M. Harmand, M. Servol, and J. C. Kieffer, “High repetition rate laser produced soft x-ray source for ultrafast x-ray absorption near edge structure measurements," Rev Sci Instrum **78**, 113104 (2007).
9. U. Shymanovich, M. Nicoul, W. Lu, S. Khle, “Toward ultrafast time-resolved Debye–Scherrer x-ray diffraction using a laser-plasma source," Rev. Sci. Instrum. **80**, 083102 (2009).
10. M. Bargheer, N. Zhavoronkov, M. Woerner and T. Elsaesser, “Recent Progress in Ultrafast X-ray Diffraction," Chemphyschem **7**, 783–792 (2006).
11. S. Kneip, C. McGuffey, J. L. Martins, S. F. Martins, C. Bellei, “Bright spatially coherent synchrotron X-rays from a table-top source," Nat. Phys. **6**, 980–983 (2010).
12. C. Spielmann, N. H. Burnett, S. Sartania, R. Koppitsch, “Generation of coherent X-rays in the water window using 5-femtosecond laser pulses," Science **278**, 661–664 (1997).
13. C. Tillman, A. Persson, C. G. Wahlström, S. Svanberg, “Imaging using hard X-rays from a laser-produced plasma," Appl. Phys. B **61**, 333–338 (1995).
14. L.-M. Chen, M. Kando, M. H. Xu, Y. T. Li, J. Koga, M. Chen, “Study of X-ray emission enhancement via a high-contrast femtosecond laser interacting with a solid foil," Phys. Rev. Lett. **100**, 045004 (2008).
15. F. Dorchies, N. Fedorov, L. Lecherbourg , “Experimental station for laser-based picosecond time-resolved x-ray absorption near-edge spectroscopy," Rev. Sci. Instrum. **86**, 073106 (2015).
16. L. Miaja-Avila, G. C. O’Neil, J. Uhlig, C. L. Cromer, “Laser plasma x-ray source for ultrafast time-resolved x-ray absorption spectroscopy," Struct. Dyn. **2**, 024301 (2015).
17. G. C. O’Neil, L. Miaja-Avila, Y. I. Joe, B. K. Alper, “Ultrafast time-resolved X-ray absorption spectroscopy of ferrioxalate photolysis with a laser plasma X-ray source and microcalorimeter array," J. Phys. Chem. Lett. **8**, 1099–1104 (2017).
18. T. Feurer, A. Morak, I. Uschmann, C. Ziener, H. Schwoerer, “Femtosecond silicon K α pulses from laser-produced plasmas," Phys. Rev. E **65**, 016412 (2001).
19. A. P. Shevelko, A. A. Antonov, I. G. Grigorieva, “Focusing crystal von Hamos spectrometer for x-ray spectroscopy and x-ray fluorescence applications," P. Soc. Photo-Opt. Ins. **4144**, 148-155 (2000).
20. M. Iqbal, Z. Urrehman, H. Im, J. G. Son, O. Seo, H. Stiel, P. V. Nickles, D. Y. Noh, “Performance improvement of a Kα source by a high-resolution thin-layer-graphite spectrometer and a polycapillary lens," Appl. Phys. B **116**, 305-311 (2014).
21. B. Ravel, M. Newville, “ATHENA, ARTEMIS, HEPHAESTUS: data analysis for X-ray absorption spectroscopy using IFEFFIT," J. Synchrotron Radiat. **12**, 537-541 (2005).
22. W. F. J. Fontijn, P. J. Van der Zaag, L. F. Feiner, “A consistent interpretation of the magneto-optical spectra of spinel type ferrites," J. Appl. Phys **85**, 5100-5105 (1999).
23. W. Fontijn, P. Van der Zaag, M. Devillers, V. Brabers, and R. Metselaar, “Optical and magneto-optical polar Kerr spectra of Fe_3O_4 and Mg^{2+} - or Al^{3+} -substituted Fe_3O_4," Phys. Rev. B **56**, 5432-5442 (1997).
24. J. Tang, M. Myers, K. A. Bosnick, L. E. Brus, “Magnetite Fe_3O_4 nanocrystals: spectroscopic observation of aqueous oxidation kinetics," J. Phys. Chem. **107**, 7501-7506 (2003).
25. A. H. De Vries, L. Hozoi, R. Broer, “Origin of the chemical shift in X-ray absorption near-edge spectroscopy at the Mn K-edge in manganese oxide compounds," Int. J. Quantum. Chem. **91**, 57-61 (2003).
26. J. Chen, H. Zhang, I. V. Tomov, M. Wolfsberg, “Transient structures and kinetics of the ferrioxalate redox reaction studied by time-resolved EXAFS, optical spectroscopy, and DFT," J. Phys. Chem. A **111**, 9326-9335 (2007).